Viscoelastic dynamics of spherical composite vesicles

S.B. Rochal, V.L. Lorman, G. Mennessier

Viscoelastic dynamics of spherical composite vesicles

S. B. Rochal,[1,2] V. L. Lorman,[1] and G. Mennessier[1]

[1]*Laboratoire de Physique Mathematique et Théorique, CNRS–Université Montpellier 2, Place Eugene Bataillon, 34095 Montpellier, France*

[2]*Physical Faculty, Rostov State University, 5 Zorge Street, 344090 Rostov-on-Don, Russia*
(Received 6 October 2003; revised manuscript received 21 October 2004; published 11 February 2005)

A micromechanical model for the low-frequency dynamics of spherical composite vesicles (CVs) is proposed. Solidlike viscoelastic properties of the CVs are taken into account. The equations of motion of a CV surrounded by a viscous liquid are derived. They have discrete solutions which describe linearly coupled stretching and bending relaxation modes and an independent shear mode. The qualitative difference between the bending modes excited in a spherical vesicle and that in a flat membrane is demonstrated. The shear elasticity of the CVs gives an essential contribution to the relaxation rate of the bending mode at small wave numbers. It is also shown that even in an incompressible spherical vesicle with a finite shear modulus, the bending mode involves both radial and tangent displacements. These reasons make both in-plane and out-of-plane low-frequency responses of the CV quite different with respect to those of the flat membrane. To compare our theoretical results with published experimental data, the power spectra of the actin-coated CV are calculated.

PACS number(s): 87.16.Dg, 82.70.Uv, 46.35.+z

I. INTRODUCTION

The response of the living cell to external perturbations is closely related to the mechanical properties of its membrane. The cell membrane consists of the phospholipid bilayer anchored to the underlying cytoskeleton which is composed of the cross-linked network of biopolymers [1]. Both the spectrin network (in red blood cells) and the actin cortex interact strongly with the bilayer and ensure cell elastic properties which prevent membrane failure during large deformations [1–4]. Thanks to recent experimental progress, one can now create *in vitro* composite systems which approach the cell membrane dynamics, namely protein-coated phospholipid vesicles [5], or vesicles coated with stiff cytoskeletal filaments [6–8]. Both the traditional micropipette method [[5], and reference therein, [9]] and a new microrheology technique [6–8] have revealed striking differences in behavior of these bio-mimetic complexes with respect to that of bare vesicles. In lipid vesicles with attached biopolymer networks, a dramatic reduction in the thermal fluctuation amplitudes is observed [5–8]. In addition, typical solidlike viscoelastic properties of the composite vesicles (CVs), including finite inplane shear and stretching moduli, have been observed [6–8]. Furthermore, a dynamical external load on a CV results in a buckling instability [8].

Conventional hydrodynamic theory [10–12] describes the dynamics of the nearly spherical vesicles with a fluid shell. The approach [10–12] is based upon the explicit constraints of constant vesicle volume and area during the shape fluctuations. The above constraints are usually justified by the principle of energy scale separation. According to this principle, if the vesicle possesses some excess area with respect to the sphere of equivalent volume, then it is much easier to bend the vesicle than to stretch it. The motion of the incompressible surrounding liquid inside and outside the vesicle is described by the Navier-Stokes equation without the inertial term. This simplification is possible [10–12] because the

Reynolds number for such a system is very small. Finally, in the equation of motion [10–12] the forces due to bending elasticity of the fluid vesicle are balanced by the viscous forces of the liquid. Therefore, the solutions of this model form the single overdamped bending branch.

In contrast to the liquid shell, the pure bending deformation of a solid shell without holes and with any nontrivial shape (including spherical and nearly spherical ones) is impossible. For geometrical reasons, bending of a spherical elastic shell is always accompanied by stretching [13]. The corresponding elastic energy of a thin solid shell differs greatly with respect to that of a fluid vesicle and explains the elastic instability of the shell [14,15]. Along the same line, the geometrical coupling between the strain components of a CV leads to a series of peculiarities in its dynamical behavior in hydrodynamic flows. A recent study [16] of a flat viscoelastic membrane has already shown the importance of shear and compression modes in the dynamics of bio-mimetic objects, emulsions, and Langmuir monolayers. However, Ref. [16] does not consider the influence of curvature on the membrane dynamics. Furthermore, its authors mention that the results obtained cannot be applied to the spherical viscoelastic membranes. The aim of the present article is to develop a linear dynamics theory for the spherical CV coupled hydrodynamically to the inner and outer viscous liquid. The paper is organized as follows. Section II is mainly devoted to the calculation of viscoelastic forces induced by a small deformation of a thin spherical shell. For this purpose the linear dynamics method is applied. Section III deals with coupled dynamics of the spherical CV and surrounding liquid. The solutions of corresponding elastohydrodynamic equations are derived. Section IV discusses the practically important limit case of an incompressible spherical shell. Power spectra of the model are calculated in Sec. V. A numerical fitting of the actin-coated vesicle dynamics and a discussion are given in the last section.

II. EQUATIONS OF MOTION OF A THIN SPHERICAL VISCOELASTIC SHELL

We limit the model to a simple two-dimensional (2D) description of the spherical CV with the energy depending on local shell density variation, local shear, and local bending. Of course, such a description does not take into account a possible relative motion of the bilayer with respect to the protein cortex or one of the monolayers with respect to another one. However, the elasticity of the lipid bilayer is much smaller than that of the cortex. In such a case, the energy scale separation principle allows a separate description of slow and fast modes. The present study deals only with the fast modes related mainly to the cortex deformation.

The physical model considered in the paper is a thin spherical viscoelastic shell. We will characterize the deformation of the shell by its strain tensor. According to the principles of the mechanics of continuous media, such a deformation is characterized by a three-component local displacement field $\mathbf{u}=(u_r,u_\theta,u_\phi)$ depending on two local angular variables θ and ϕ. This displacement field can be expressed in Cartesian coordinates as

$$u_x = u_r\sin\theta\cos\phi + u_\theta\cos\theta\cos\phi - u_\phi\sin\phi,$$

$$u_y = u_r\sin\theta\sin\phi + u_\theta\cos\theta\sin\phi + u_\phi\cos\phi,$$

$$u_z = u_r\cos\theta - u_\theta\sin\theta. \qquad (1)$$

Equation $\mathbf{R}'=\mathbf{R}^0+\mathbf{u}$ relates the initial Cartesian coordinates $(R\sin\theta\cos\phi, R\sin\theta\sin\phi, R\cos\theta)$ of a material point $\mathbf{R}^0$

on the equilibrium sphere surface with its final coordinates $\mathbf{R}'$ in the deformed state. The final positions of all points given by the dependence $\mathbf{R}'(\theta,\phi)$ determine the shape of the deformed shell. Then, the simplest way to introduce the strain tensor is to express it in terms of the metric tensor of the surface. On the one hand, following Landau [13] (see also [17]), the squared distance dl'^2 between two infinitely close points on the deformed shell surface is expressed as

$$dl'^2 = dl_0^2 + 2\epsilon_{ij}\delta l_i\delta l_j, \qquad (2)$$

where $dl_0^2=\delta_{ij}\delta l_i\delta l_j$ is the squared distance between the same points in the initial state, ϵ_{ij} is the strain tensor, and $\delta l_1 = \delta l_\phi = R\sin\theta d\phi$ and $\delta l_2=\delta l_\theta=Rd\theta$ are the distances along the meridian (θ direction) and parallel (ϕ direction) of the sphere. On the other hand, the squared distance dl'^2 defines a metric tensor $\hat{g}(\theta,\phi,\mathbf{u}): dl'^2=g_{ij}dv_idv_j$, where $dv_1=d\phi$ and $dv_2=d\theta$ [18], tensor $\hat{g}$ being dependent on field (1). Finally, the strain tensor ϵ_{ij} can be constructed from the normalized metric tensor in the form

$$\epsilon_{ij} = \frac{1}{2}(\gamma_{ik}g_{kl}\gamma_{lj} - \delta_{ij}), \qquad (3)$$

where $\hat{\gamma}=(\hat{g}_0)^{-1/2}$ is the normalization, $\hat{g}_0$ is the metric tensor of the undeformed sphere, and δ_{ij} is the Kronecker symbol. In the explicit form $\gamma_{12}=\gamma_{21}=0$, $\gamma_{11}=(R\sin\theta)^{-1}$ and $\gamma_{22}=(R)^{-1}$. In the linear dynamics approximation (studied in the present article), the strain is considered to be small. Thus, the nonlinear terms of the strain tensor are neglected and its linear part takes the following form:

$$\hat{\epsilon} = \frac{1}{R}\begin{vmatrix} \partial_\phi u_\phi/\sin\theta + u_r + u_\theta\mathrm{ctg}\,\theta & (\partial_\phi u_\theta/\sin\theta + \partial_\theta u_\phi - u_\phi\mathrm{ctg}\,\theta)/2 \\ (\partial_\phi u_\theta/\sin\theta + \partial_\theta u_\phi - u_\phi\mathrm{ctg}\,\theta)/2 & \partial_\theta u_\theta + u_r \end{vmatrix}, \qquad (4)$$

where ∂_ϕ and ∂_θ stand for the derivatives with respect to the angular variables.

The geometrical meaning of the components of tensor (4) is similar to that of an ordinary 2D symmetrical tensor characterizing the planar strain. In particular, $\rho'/\rho_s=-\epsilon_{ii}= -\mathrm{div}\,\mathbf{u}$, where ρ' is the local density variation and ρ_s is the average density of the shell. Then the quadratic (with respect to the field $\mathbf{u}$ components) elastic energy per unit shell area can be expressed as

$$E_d = \lambda/2(\epsilon_{ii})^2 + \mu\epsilon_{ij}^2 + K/2(2u_rR^{-2} + \Delta_s u_r)^2, \qquad (5)$$

where λ and μ are the in-plane elastic moduli analogous to Lame coefficients in the 3D case [13]. The first two terms in energy (5) are constructed as the invariants of tensor (4) and have the form widely used in the mechanics of elastic solids [13]. These two contributions can also be expressed in terms of two eigenvalues ϵ_1 and ϵ_2 of tensor (4): $(\epsilon_{ii})^2=(\epsilon_1+\epsilon_2)^2$ and $\epsilon_{ij}^2=\epsilon_1^2+\epsilon_2^2$. The last term in the energy expression takes into account the possibility of bending deformation. In this

term, Δ_s is the projection of the Laplacian Δ upon the sphere surface,

$$\Delta_s = \frac{1}{R^2\sin^2\theta}\partial_\phi^2 + \frac{1}{R^2}\partial_\theta^2 + \frac{\mathrm{ctg}\,\theta}{R^2}\partial_\theta. \qquad (6)$$

Coefficient K stands for the bending rigidity. For small deformation, the linear part of the mean curvature deviation from the equilibrium value $2/R-1/R_1-1/R_2$ is $2u_rR^{-2}+\Delta_s u_r$, where R_1 and R_2 are the principal curvature radii.

Energy (5) is quite similar to that used in Ref. [16] but the expressions of strain tensor and of the mean curvature deviation in Ref. [16] are different since the equilibrium curvature of the flat membrane is zero. Furthermore, inner and outer regions separated by the sphere surface are not equivalent. The local symmetry $C_{\infty v}$ of a point on the sphere surface is lower than the local symmetry $D_{\infty h}$ of a point on the plane surface. Consequently, elastic energy of the spherical membrane may contain additional terms forbidden by the symmetry of the plane membrane. Here, for the sake of clarity, we

consider the simplest form of the elastic energy which provides a description of the linear dynamics of CVs with solidlike properties.

The quadratic part of the elastic energy determines completely the linear dynamics but is not sufficient to describe the spontaneous variation of the equilibrium shape. The simplest energy valid for the shape transition description should include at least fourth-order terms. A model containing fourth-degree terms in local principal stretches λ_i has been proposed in Ref. [19] to simulate numerically the shape transitions in red blood cells. The local principal stretches λ_i [19] are related to eigenvalues ϵ_1 and ϵ_2 of strain tensor (4) in the following way: $\epsilon_i = (\lambda_i^2 - 1)/2$. In the case of the small strain, this relation takes the form $\epsilon_i = \lambda_i - 1$. The quadratic part of energy [19] coincides with energy (5) up to the coefficient notations. Namely, the coefficients k_b, K_α, and μ from Ref. [19] should be replaced by K, λ, and $\mu - \lambda$ from the present work. The analytical description of the shape transition is outside the framework of this paper.

We divide the derivation of the equations of motion for the viscoelastic CV coupled with the surrounding liquid into two steps. First, the equations of motion of an empty elastic shell are deduced in order to evaluate the elastic forces acting in the system and to perform the symmetry analysis of the modes. Second, these equations are modified by taking into account internal and external nonelastic forces induced by the internal viscosity of the shell and by the interaction between the shell and the surrounding liquid, respectively. The first step can be completely performed within the frame of the action minimization approach. The action in the developed model reads

$$A = R^2 \iiint \left[\rho_s(\dot{\mathbf{u}})^2/2 - E_d \right] \sin\theta d\theta d\phi dt, \tag{7}$$

where $\dot{\mathbf{u}} = \partial_t \mathbf{u}$ is the velocity of the shell.

Formal minimization of the action with respect to the function $\mathbf{u}(\theta, \phi, t)$ gives three equations of motion corresponding to the three components of the field $\mathbf{u}$,

$$\rho_s \ddot{u}_r = -\frac{\partial E_d}{\partial u_r} + \frac{d}{\sin\theta d\theta}\frac{\partial(E_d \sin\theta)}{\partial(\partial u_r/\partial\theta)} - \frac{d^2}{\sin\theta d\theta^2}\frac{\partial(E_d \sin\theta)}{\partial(\partial^2 u_r/\partial\theta^2)}$$
$$- \frac{d^2}{d\phi^2}\frac{\partial(E_d)}{\partial(\partial^2 u_r/\partial\phi^2)},$$

$$\rho_s \ddot{u}_\theta = -\frac{\partial E_d}{\partial u_\theta} + \frac{d}{\sin\theta d\theta}\frac{\partial(E_d \sin\theta)}{\partial(\partial u_\theta/\partial\theta)} + \frac{d}{d\phi}\frac{\partial(E_d)}{\partial(\partial u_\theta/\partial\phi)},$$

$$\rho_s \ddot{u}_\phi = -\frac{\partial E_d}{\partial u_\theta} + \frac{d}{\sin\theta d\theta}\frac{\partial(E_d \sin\theta)}{\partial(\partial u_\phi/\partial\theta)} + \frac{d}{d\phi}\frac{\partial(E_d)}{\partial(\partial u_\phi/\partial\phi)}. \tag{8}$$

The right-hand terms in Eqs. (8) express the elastic forces acting on the unit area of the shell. The structure of the first equation in system (8) differs from that of the two other equations since energy (5) contains second-order derivatives of the u_r component and does not contain terms with $\partial_\phi u_r$ derivative. The explicit form of system (8) is given below,

$$\rho_s \ddot{u}_r = -\frac{2(\lambda + \mu)}{R}\text{div } \mathbf{u} - K\left(\frac{2}{R^2} + \Delta_s\right)^2 u_r,$$

$$\rho_s \ddot{u}_\theta = \mu\{\Delta_s u_\theta + [u_\theta(1 - 2\cos^2\theta) - 2\cos\theta\partial_\phi u_\phi]/(R^2\sin^2\theta)\}$$
$$+ \frac{(\lambda + \mu)}{R^2\sin\theta}(-\text{ctg }\theta\partial_\phi u_\phi + \partial^2_{\phi,\theta}u_\phi + \cos\theta\partial_\theta u_\theta - u_\theta/\sin\theta$$
$$+ 2\sin\theta\partial_\theta u_r + \sin\theta\partial^2_{\theta\theta}u_\theta),$$

$$\rho_s \ddot{u}_\phi = \mu\{\Delta_s u_\phi + [u_\phi(1 - 2\cos^2\theta) + 2\cos\theta\partial_\phi u_\theta]/(R^2\sin^2\theta)\}$$
$$+ \frac{(\lambda + \mu)}{R^2\sin\theta}(\text{ctg }\theta\partial_\phi u_\theta + \partial^2_{\phi,\theta}u_\theta + 2\partial_\phi u_r + \partial^2_{\phi\phi}u_\phi/\sin\theta). \tag{9}$$

To obtain the solution of system (9), we use the usual methods of linear dynamics. The complete description of these methods can be found elsewhere [20]. Here we recall several basic ideas only. In the linear approximation, each mode spans one irreducible representation (IR) of the symmetry group of the system. The corresponding solution of the equation of motion is the basis function of this IR. For several mutually independent basis functions of the same IR, the solution (normal mode) is their linear combination. In other words, the modes of the same symmetry are linearly coupled. Following this general procedure, we have to investigate the symmetry properties of the displacement field (i.e., to determine the list of active IRs of the sphere symmetry group O_3 and to deduce the explicit form of their basis functions spanning the displacement field). The direct product $(D_0[1] + D_1[-1] + D_2[1] \cdots) \times V$ contains all possible irreducible displacement fields. Corresponding basis functions result from its projection onto IRs. Here $D_l[\text{Pr}]$ are the IRs spanned by well-known spherical harmonics $Y_{lm}(\theta, \phi)$ with parity $\text{Pr} = (-1)^l$, where l is the IR index ($l \geq 0$). The basis function index m changes from $-l$ to l. The basis functions of the IR V are three components of a conventional vector: $V = D_1[-1]$. The functions resulting from the projection procedure determine the direction and the amplitude of the irreducible displacement field in the point specified by the angular coordinates (θ, ϕ).

Finally, the radial displacement field $\mathbf{u}_\perp$ (usually associated with bending deformation) of the shell can be presented as a linear combination of $Y_{lm}(\theta, \phi)$ functions,

$$\mathbf{u}_\perp = \sum_{l=0}^{l=\infty} \sum_{m=-l}^{m=l} A_{lm}^Y Y_{lm}(\theta, \phi)\mathbf{e}_r, \tag{10}$$

where $\mathbf{e}_r$ is the radial unit vector in a spherical coordinate system. A tangent displacement field can be expressed in terms of $\mathbf{Z}_{lm}(\theta, \phi)$ and $\mathbf{W}_{lm}(\theta, \phi)$ functions describing stretching and shear fields, respectively,

$$\mathbf{u}_\parallel = \sum_{l=1}^{l=\infty} \sum_{m=-l}^{m=l} [A_{lm}^Z \mathbf{Z}_{lm}(\theta, \phi) + A_{lm}^W \mathbf{W}_{lm}(\theta, \phi)]. \tag{11}$$

Here $\mathbf{Z}_{lm}(\theta, \phi)$ and $\mathbf{W}_{lm}(\theta, \phi)$ are vector spherical harmonics detailed in the Appendix. Note that functions $\mathbf{Z}_{lm}$ and Y_{lm} with the same l span the same IR. Therefore, the bending mode (with $l > 1$) conventionally associated with radial displacements only always involves the local density variation, or stretching (see Fig. 1). The parity $\text{Pr} = (-1)^{(l+1)}$ of the
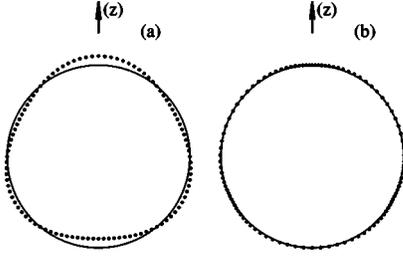
FIG. 1. Radial (a) and tangent (b) distortions of a spherical shell having the same symmetry. The corresponding displacement fields Y_{30} (a) and $\mathbf{Z}_{30}$ (b) span $D_3[-1]$ representation of the O_3 symmetry group. The vertical direction coincides with the z axis.

"shear" functions $\mathbf{W}_{lm}$ is different from that of Y_{lm} or $\mathbf{Z}_{lm}$. Therefore, the stretching and bending modes do not interact linearly with the shear one, making the shear mode independent.

Consequently, the normal mode with the indices l and m and the symmetry of coupled bending and stretching modes is a linear combination of two functions: $Y_{lm}(\theta, \phi)\mathbf{e}_r$ and $\mathbf{Z}_{lm}(\theta, \phi)$. To obtain the secular equation of the system and the dispersion relation of the bending-stretching mode, we substitute the components of vector

$$\mathbf{u} = \left[\mathbf{e}_r A_{lm}^Y Y_{lm}(\theta, \phi) + A_{lm}^Z \mathbf{Z}_{lm}(\theta, \phi)\right]\exp(-i\omega t) \quad (12)$$

with an unknown ratio between two amplitudes A_{lm}^Y and A_{lm}^Z into system (9). It results in a linear homogeneous system with respect to A_{lm}^Y and A_{lm}^Z coefficients,

$$(L_{11} - \rho_s\omega^2)A_{lm}^Y + L_{12}A_{lm}^Z = 0,$$

$$L_{21}A_{lm}^Y + (L_{22} - \rho_s\omega^2)A_{lm}^Z = 0, \quad (13)$$

where

$$\hat{L} = \begin{vmatrix} 4\dfrac{(\lambda + \mu)}{R^2} + \dfrac{K(l^2 + l - 2)^2}{R^4} & -2\dfrac{(\lambda + \mu)\sqrt{l(l+1)}}{R^2} \\[2ex] -2\dfrac{(\lambda + \mu)\sqrt{l(l+1)}}{R^2} & \dfrac{(\lambda + \mu)l(l+1) + \mu(l^2 + l - 2)}{R^2} \end{vmatrix}. \quad (14)$$

The matrix $\hat{L}$ is independent of m value since solutions with the same l and different m are equivalent. The system has a solution if its determinant is equal to zero. For each $l > 0$, this condition determines simultaneously two frequencies for both coupled bending-stretching modes (the frequency becomes single only in the case $l=0$; its value can be deduced from equation $\rho_s\omega^2 = L_{11}$). The number of equivalent solutions (with the same dispersion law) is equal to the dimension of the corresponding IR. Though each resulting mode contains both radial and tangent components, the contribution of the fields (given by the ratio A_{lm}^Y/A_{lm}^Z) is quite different. One of the modes has a big tangent and a small radial contribution and can be conventionally called the "nearly stretching mode." The nearly stretching mode involves the displacements inducing the local-density variation. Another mode has a big radial and a small tangent amplitude and is called the "nearly bending mode." Its frequency in the case $l=1$ is equal to zero since the corresponding deformation field coincides with a simple shell translation.

Analogously, the shear-type solution can be obtained by substitution of vector $\mathbf{u}'$ components

$$\mathbf{u}' = A_{lm}^W \mathbf{W}_{lm}(\theta, \phi)\exp(-i\omega t) \quad (15)$$

into system (9). The dispersion relation of the shear mode has the form

$$\rho_s\omega^2 = \mu(l - 1)(l + 2)/R^2. \quad (16)$$

The solution with $l=1$ and $m=0$ is the simple shell rotation about the z axis.

In the following step, we take into account the dissipation in the system. The dissipation takes place both in the shell and in the liquid. For giant fluid vesicles, the dominant dissipation occurs in the surrounding fluid [12]. Internal membrane friction and permeation through the membrane can be neglected. Composite vesicles can still be considered as impermeable for liquid but their internal friction becomes relevant. Taking into account internal friction forces modifies the equations of motion obtained and the corresponding dispersion relations. In the low-frequency limit, the shell dissipation function has a form which coincides with energy (5) up to the substitution $\mathbf{u} \rightarrow \partial_t\mathbf{u}$ and up to the coefficients notation. The same substitution converts the elastic terms in the equations of motion into the viscous ones. As a consequence, the contribution of the internal friction modifies Eqs. (13), (14), and (16) as follows: $\lambda \rightarrow \bar{\lambda} = \lambda - i\xi_s\omega, \mu \rightarrow \bar{\mu} = \mu - i\eta_s\omega$, and $K \rightarrow \bar{K} = K - iK_f\omega$, where η_s is the ordinary [7] in-plane shear viscosity of the shell. In-plane viscosity ξ_s is associated with the velocity of the relative area variation. Coefficient K_f stands for the viscosity related to the velocity of bending deformation. In the higher-frequency region, the shell dissipation function will include the high-order time derivatives of the displacement field. Consequently, the viscoelastic moduli will have the form $\bar{\lambda} = \Sigma_{n=0}^{n=\infty} G_n^\lambda (-i\omega)^n, \bar{\mu} = \Sigma_{n=0}^{n=\infty} G_n^\mu (-i\omega)^n$, and $\bar{K} = \Sigma_{n=0}^{n=\infty} G_n^K (-i\omega)^n$ and will replace λ, μ, and K in matrix (14) and Eq. (16). The stability of the shell and the energy dissipation during the time course impose additional conditions to coefficients G_n^j.

III. EXTERNAL FORCES DUE TO SURROUNDING LIQUID AND THEIR CONTRIBUTION TO THE EQUATIONS OF MOTION

External forces due to dissipation in the surrounding viscous liquid influence strongly the modes of CVs. In the frame of the proposed model, they lead to a further modification of the solutions of system (9). The dynamics of an incompressible liquid is described by the Navier-Stokes equation,

$$\rho_h \frac{d\mathbf{v}}{dt} = - \nabla p_h + \eta \Delta \mathbf{v}, \qquad (17)$$

where p_h is the hydrostatic pressure, and ρ_h, η, and $\mathbf{v}$ denote the density, shear viscosity, and the velocity of the liquid, respectively. Due to the very small Reynolds number calculated for vesicles in water flow [11,12], the left part of Eq. (17) is usually assumed to be negligible. For the same reason, the ρ_s value in Eqs. (9) can also be neglected. Nevertheless, it is obvious that the above assumptions are valid in the low-frequency region only. The relative contribution of the inertial term increases with frequency. For oscillation processes, the inertial and viscous terms of Eq. (17) can be estimated as $\rho_h \omega^2 u_s$ and $\eta \omega u_s / R^2$, respectively, where u_s is the vibration amplitude. For vesicles with $R \approx 15$–20 μm and an embedding liquid with $\eta \approx 10^{-3}$ Pa s and $\rho_h \approx 10^3$ kg/m^3, the contribution of the inertial terms may become essential at frequencies higher than ≈ 10 kHz.

The solutions of Eq. (17) allow us to calculate the viscous stress tensors σ_{ij} (see Ref. [21]) at both surfaces of the vesicle. To determine the inner and outer external forces acting upon a unit area of the vesicle, the corresponding tensors σ_{ij} are multiplied by the outer and inner normal vectors. Then external forces Π_i are added to the right parts of the corresponding equations of system (9),

$$\Pi_r = \sigma_{rr}^{in} - \sigma_{rr}^{out}, \quad \Pi_\theta = \sigma_{r\theta}^{in} - \sigma_{r\theta}^{out}, \Pi_\phi = \sigma_{r\phi}^{in} - \sigma_{r\phi}^{out}, \quad (18)$$

where the relevant components of tensor σ_{ij} read

$$\sigma_{rr} = - p_h + 2\eta \partial_r v_r,$$

$$\sigma_{r\theta} = \eta[(\partial_\theta v_r)/r + \partial_r v_\theta - v_\theta/r],$$

$$\sigma_{r\theta} = \eta[\partial_r v_\phi + (\partial_\phi v_r)/(r \sin \theta) - v_\phi/r]. \qquad (19)$$

Here r is the radial variable in the spherical coordinate system. Besides, following Landau and Lifchitz [21], we assume that both the inner and the outer velocities of the liquid at the shell surface $\mathbf{v}_{surf}^{in}$ and $\mathbf{v}_{surf}^{out}$ are equal to the velocity $\dot{\mathbf{u}}$ of the shell. These boundary conditions are the last contributions to the elastohydrodynamical model, which determines the dynamics of a CV in the surrounding liquid. They relate Eq. (17), completed with mass conservation law $\nabla \cdot \mathbf{v} = 0$ on the one hand, and system (9) modified by taking into account the internal and external forces on the other hand.

The relaxation limit of Eq. (17) with the boundary conditions defined on a sphere has been considered by Lamb [22]. The irreducible solution valid for the region inside the vesicle and compatible with the coupled bending and stretching modes reads

$$p_h = B_{lm}^{in}[(r/R)^l]Y_{lm},$$

$$\mathbf{v} = \left[A_{lm}^{in} l \frac{r^{l-1}}{R^l} + B_{lm}^{in} \frac{lr^{l+1}}{2\eta(2l+3)R^l} \right] Y_{lm} \mathbf{e}_r$$
$$+ \left[A_{lm}^{in} \frac{r^{l-1}}{R^l} + B_{lm}^{in} \frac{(l+3)r^{l+1}}{2\eta(l+1)(2l+3)R^l} \right] \mathbf{Z}_{lm} \sqrt{l(l+1)}.$$
$$(20)$$

The velocity $\mathbf{v}$ in Eq. (20) satisfies also the mass conservation law. The solution for the outer liquid is obtained from Eq. (20) by the substitution $l \to -(l+1)$ performed in square brackets only and by the change in constants notations. Except for notation, Eqs. (20) coincide with those given by Lenz and Nelson in the appendix to Ref. [23]. The constants $A_{lm}^{in}, B_{lm}^{in}, A_{lm}^{out},$ and B_{lm}^{out} are determined from the boundary conditions formulated above. At the shell surface ($r=R$), the amplitude $\mathbf{v}_0(r)$ of the liquid velocity in Eq. (20) is equal to $-i\omega \mathbf{u}_0$, where $\mathbf{u}_0$ is the amplitude of the shell displacement field (12). The unknown coefficients in Eq. (20) can be expressed in terms of the shell displacement field amplitudes A_{lm}^Y and A_{lm}^Z using this equality. External forces (18) bring in an additional contribution which modifies system (13). Namely, the following matrix $\hat{Q}$ should be added to matrix $\hat{L}$ [see Eqs. (13) and (14)]:

$$\hat{Q} = \frac{-i\omega}{R} \begin{vmatrix} \eta_{in} \frac{2l^2+l+3}{l} + \eta_{out} \frac{2l^2+3l+4}{l+1} & -3\eta_{in} \sqrt{\frac{l+1}{l}} - 3\eta_{out} \sqrt{\frac{l}{l+1}} \\ -3\eta_{in} \sqrt{\frac{l+1}{l}} - 3\eta_{out} \sqrt{\frac{l}{l+1}} & \eta_{in}(2l+1) + \eta_{out}(2l+1) \end{vmatrix}. \qquad (21)$$

The matrix $\hat{Q}$ relates the amplitudes of the shell displacement A_{lm}^Y and A_{lm}^Z to the corresponding amplitudes of external normal and tangential forces (18). For living cells and in many cases for artificial vesicles and membranes (see, for example, Ref. [16]), outside and inside viscosities η_{out} and η_{in} of the surrounding liquids are different. Matrix $\hat{Q}$ takes this fact into account. In some other cases, the inner and the outer region of the shell may contain the same liquid with the viscosity $\eta = \eta_{out} = \eta_{in}$. Then matrix $\hat{Q}$ is simplified to the form

$$\hat{Q}' = \begin{vmatrix} -\dfrac{i\omega\eta(2l+1)(2l^2+2l+3)}{l(l+1)R} & \dfrac{3i\omega\eta(2l+1)}{\sqrt{l(l+1)}R} \\ \dfrac{3i\omega\eta(2l+1)}{\sqrt{l(l+1)}R} & -\dfrac{2i\omega\eta(2l+1)}{R} \end{vmatrix}.$$

$$(22)$$

Final secular equations of the bending and stretching modes of the shell in the liquid become

$$(\hat{L} + \hat{Q})\mathbf{u}_0 = 0, \qquad (23)$$

where $\mathbf{u}_0 = (A_{lm}^Y, A_{lm}^Z)$ is the amplitude of the displacement field (12) and $\hat{L} = \hat{L}(\bar{\lambda}, \bar{\mu}, \bar{K})$ is expressed in terms of viscoelastic moduli in order to take into account the internal friction in the shell. Then, the dynamical equation

$$\det\left|\hat{L} + \hat{Q}\right| = 0 \qquad (24)$$

defines simultaneously two overdamped dispersion laws $\omega(l)$ for both modes.

Similar considerations applied to the case of the shear mode modify its dispersion relation (16). The irreducible solution of the Navier-Stokes equation with the appropriate symmetry reads

$$p_h^{\text{in}} = 0; \quad p_h^{\text{out}} = 0; \quad \mathbf{v}^{\text{in}} = \left[C_{lm}^{\text{in}} \frac{r^l}{R^l} \right] \mathbf{W}_{lm};$$

$$\mathbf{v}^{\text{out}} = \left[C_{lm}^{\text{out}} \frac{R^{l+1}}{r^{l+1}} \right] \mathbf{W}_{lm}. \qquad (25)$$

With the contribution of external viscous forces (18), the modified shear mode dispersion relation takes the form

$$\bar{\mu}(l-1)(l+2)/R^2 - i\omega[\eta_{\text{in}}(l-1) + \eta_{\text{out}}(l+2)]/R = 0. \qquad (26)$$

Hydrodynamic flow fields arising around the spherical vesicle and associated with modes of different types are shown in Fig. 2.

As an additional remark, let us note that the dispersion relations of the flat membrane (see [16] and references therein) can be reproduced as a simplified particular case of Eqs. (24) and (26). For this purpose, it is sufficient to substitute $l = qR$, where q is the mode wave vector and then to take the $R \to \infty$ limit. More details of the spherical vesicle dynamics (compared to that of the flat membrane) are given in Sec. IV. In this section, the case of the incompressible shell is considered for two reasons. First, it simplifies the description and makes the comparison easy. Second, the incompressible shell approximation is extensively used for the fitting of microrheological experimental data on actin-coated vesicles [6–8].

IV. BENDING MODE IN THE INCOMPRESSIBLE SPHERICAL SHELL

Let us first clarify the concept of the incompressible spherical shell. If this concept means that the shell area is

strictly constant, then only the shear mode is possible in the spherical vesicle dynamics. This geometrical understanding of the problem appears unsuitable for the viscoelastic shell from the physical point of view. Completely incompressible solids and liquids do not exist in nature. It is more convenient to assume that the compressibility λ [see energy (5)] is much greater than the other elastic coefficients. Then, the limit $\lambda \to \infty$ constitutes the incompressible shell approximation which satisfies the local incompressibility condition div $\mathbf{u} = 0$.

To obtain the dispersion relation of the bending mode for the incompressible shell, we come back to the analysis of Eq. (24). Note that this equation is linear with respect to $\bar{\lambda}$. We divide Eq. (24) by $\bar{\lambda}$ (it is possible since $\bar{\lambda} \neq 0$) and then calculate the $\lambda \to \infty$ limit. Instead of two possible coupled modes in a compressible shell, it gives the single mode with the dispersion relation

$$\omega = -i(l^2 + l - 2) \frac{\bar{K}l(l+1)(l^2+l-2) + 4R^2\bar{\mu}}{R^3 \eta(2l+1)(2l^2+2l-1)}, \qquad (27)$$

where $l > 1$. The case $l = 1$ represents a simple shell translation. Here, for the sake of clarity, we consider inner and outer liquids identical; viscosity η denotes $\eta_{\text{out}} = \eta_{\text{in}} = \eta$. The mode obtained describes a bending deformation of the shell, though it contains both radial and tangent contributions with a fixed amplitudes ratio. The polarization of the mode can be found from system (23). With that aim, we divide the matrix of the system by $\bar{\lambda}$ and take the $\lambda \to \infty$ limit. This simple calculation shows that the ratio A_{lm}^Y/A_{lm}^Z between the radial and tangent amplitudes of the displacement field is $\sqrt{l(l+1)}/2$. The mode with this ratio satisfies automatically the linear incompressibility condition div $\mathbf{u} = 0$. Let us stress that the purely radial displacement field, extensively discussed in the literature, always leads to a local shell density variation or stretching. Furthermore, this effect is linear in the displacement field amplitude. Though a purely radial displacement with $l > 0$ does not give a linear contribution to the total area variation, the local area changes are of the first order in u_r. For the whole shell, the extension in regions with $u_r > 0$ is compensated by the compression in regions with $u_r < 0$. To satisfy the div $\mathbf{u} = 0$ condition, the displacement field should possess both radial and tangent components. Note also that the linear incompressibility condition does not mean that the total shell area is strictly constant. It means that the local area change is of second order in the displacement field amplitude. Therefore, the real spherical shell with an extremely big λ value can undergo a total area change. But this variation cannot contain terms linear in the displacement field amplitude. Finally, the linear dynamics of a spherical incompressible shell is characterized by two modes: one in-plane shear mode with dispersion relation (26) and bending mode (27) involving both radial and tangent displacements.

Consideration of the limit case of an incompressible membrane simplifies the basic formulas of the model and clearly demonstrates the qualitative difference between the bending mode excited in the spherical vesicle and that in the
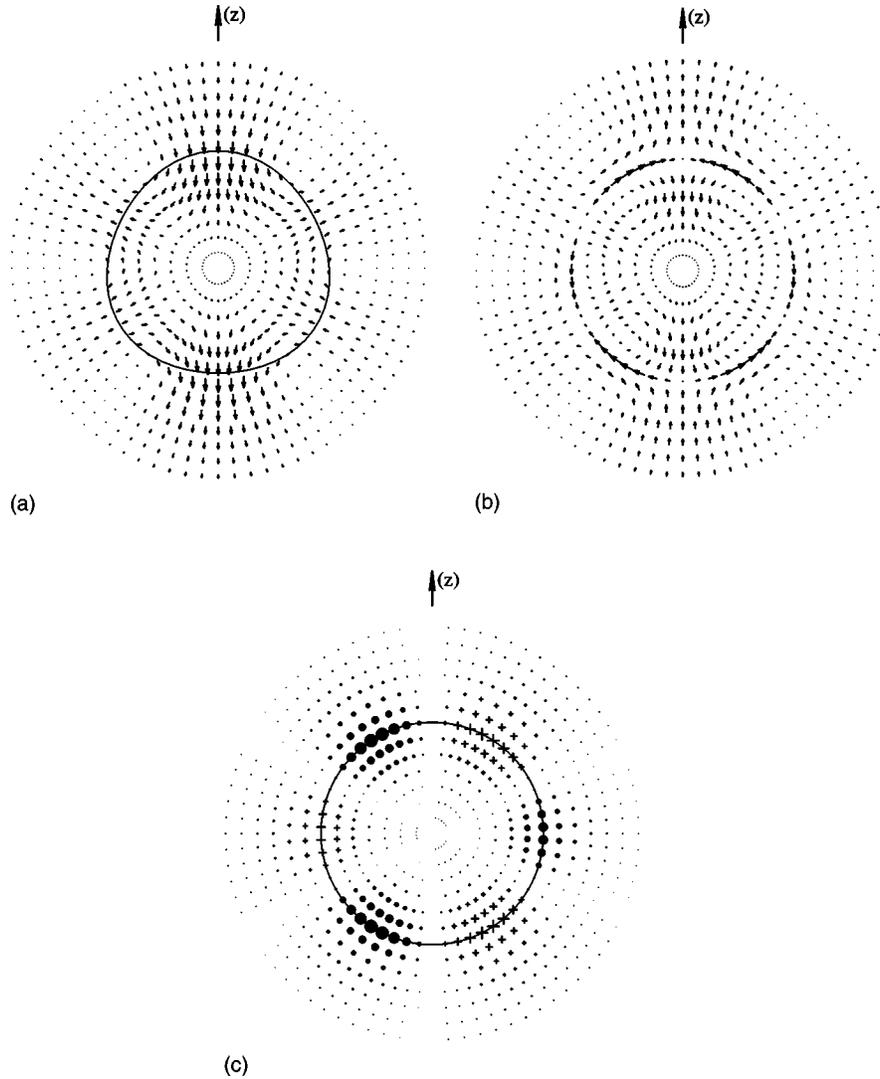
FIG. 2. Hydrodynamic flow fields around a spherical vesicle. 2D sections by the plane containing the z axis are shown. The three different modes presented are characterized by the same indices $l=3$ and $m=0$. Since $m=0$, the hydrodynamic flows (a)–(c) have rotational symmetry about the z direction. According to the conventional boundary condition, the velocity of the membrane surface $\dot{\mathbf{u}}$ is equal to the velocity $\mathbf{v}$ of liquid at the vesicle surface. Due to the overdamped character of the possible modes $\mathbf{u}=-\tau\mathbf{v}$, where the mode frequency ω is related to its relaxation time τ as $\tau=-i/\omega$. (a) Bending mode. The current vesicle shape shown by the solid line is different from the equilibrium spherical one. The ratio between the radial and tangent components of the hydrodynamic flow corresponds to the case of an incompressible membrane (see in the text). (b) Stretching mode. The deviation from the spherical shape of the vesicle induced by this mode is not significant since the ratio between radial and tangent components of the shell displacement field $\mathbf{u}$ is small. Consequently, the hydrodynamic flow at the vesicle surface is almost tangent to it. For the sake of clarity, the solid line of the shell surface is omitted. (c) Shear mode leads only to in-plane deformation of the spherical membrane. Spherical vesicle shape is shown by the solid line. Hydrodynamic flow is perpendicular to the plane of the figure. Two opposite directions of the flow are shown by crosses and full circles. Their size is proportional to the flow velocity.

flat membrane (FM). First, the bending mode of the spherical vesicle always involves the in-plane displacement. Second, the shear modulus $\bar{\mu}$ contributes to its relaxation rate. Both effects are greater in the region of small l value, where the spherical geometry strongly influences the dispersion laws (24), (26), and (27).

As an additional remark, let us note that the classical result [11,12] for the bending mode dynamics in a nearly spherical fluid vesicle can be obtained as a particular case $\bar{\mu}=0$ of the simplified incompressible shell dynamics [Eq. (27)]. More precisely, in the Milner and Safran formulas [11]

the following substitution should be made: $\gamma=0$ and $r_0/r_s=1$, where γ is the Langrange multiplier, r_0 is an equivalent-volume sphere radius, and r_s is the spontaneous curvature radius.

V. POWER SPECTRA OF THE PROBE PARTICLES

To compare the model with published experimental data [6–8], we calculate in-plane and out-of-plane power spectra $\langle x_i^2(\omega)\rangle$ of the spherical viscoelastic vesicle, where $x_i(t)$ is the probe particle (PP) position in time, $x_i(\omega)$ is its Fourier trans-

form, and $i = \|, \perp$. The PP is embedded in the vesicle and the frequency dependence of the viscoelastic moduli can be calculated from direct optical observation of in-plane and out-of-plane thermal fluctuations of the PP. Let us stress that current microrheological analyses use the results obtained for *flat* membranes to calculate the elastic constants for *spherical* CVs (see, for example, [6,7]).

By the fluctuation-dissipation theorem, the $\langle x_i^2(\omega) \rangle$ spectra can be easily expressed in terms of the response functions $\alpha_\|(\omega)$ and $\alpha_\perp(\omega)$ [16],

$$\langle x_i^2(\omega) \rangle = 2 \, \mathrm{Im}\big[\alpha_i(\omega)\big] k_B T/\omega. \quad (28)$$

Let us recall that the response α_i determines the amplitude $A_i(\omega)$ of the PP displacement when the external exciting force $F_i = F_i^0 \exp(i\omega t)$ is applied to the PP: $\alpha_i = A_i/F_i^0$. Radial response to the in-plane force or in-plane response to the radial force in the point of force application are forbidden by the symmetry of the system. To calculate the response α_i, the tangent and normal forces acting on the PP located at $\Omega^0 = (\theta^0, \phi^0)$ should be presented in terms of $\mathbf{W}_{lm}, \mathbf{Z}_{lm}$, and Y_{lm} functions. The force applied to the point is equivalent to the pressure of a δ-function character. The pressures $\mathbf{P}_\|(\Omega)$ and $P_\perp(\Omega)$ on the CV surface have the form $P_\perp(\Omega) = F_\perp^0 \delta(\Omega, \Omega^0)$ and $\mathbf{P}_\|(\Omega) = F_\|^0 \delta_\mathbf{N}(\Omega, \Omega^0)$, where $\mathbf{N}$ is the unit in-plane vector parallel to the tangent component of the applied force,

$$\delta(\Omega, \Omega^0) = \sum_{l,m} Y_{lm}(\Omega) Y_{lm}^*(\Omega^0)/R^2 \quad (29)$$

and

$$\delta_\mathbf{N}(\Omega, \Omega^0) = \sum_{l,m} \Big\{ \mathbf{Z}_{lm}(\Omega)[\mathbf{N}\mathbf{Z}_{lm}^*(\Omega^0)] + \mathbf{W}_{lm}(\Omega) \\ \times [\mathbf{N}\mathbf{W}_{lm}^*(\Omega^0)] \Big\}/R^2. \quad (30)$$

Function $\delta(\Omega, \Omega^0)$ is quite similar to the ordinary δ function, i.e., $\int \delta(\Omega, \Omega^0)dS = R^2 \int \delta(\Omega, \Omega^0)d\Omega = 1$, where dS is an element of the sphere area. Function $\delta_\mathbf{N}(\Omega, \Omega^0)$ is normalized in a slightly different way: $\int \delta_\mathbf{N}(\Omega, \Omega^0)dS = \mathbf{N}$. Besides, it is useful to note that

$$R^2 \int \delta_\mathbf{N}(\Omega, \Omega^0)\mathbf{\Psi}(\Omega)d\Omega = \mathbf{N}\mathbf{\Psi}^*(\Omega^0), \quad (31)$$

where $\mathbf{\Psi}(\Omega)$ is an arbitrary in-plane vector function.

Thanks to the explicit form of delta functions $\delta(\Omega, \Omega^0)$ and $\delta_\mathbf{N}(\Omega, \Omega^0)$, the pressure $P_\perp$ can be expanded in scalar spherical harmonics Y_{lm} and the pressure $\mathbf{P}_\|$ in vector spherical harmonics $\mathbf{Z}_{lm}$ and $\mathbf{W}_{lm}$. Then for the new balance of forces, the amplitudes of the exciting pressure harmonics should be equilibrated by the amplitudes of harmonics of internal viscoelastic and external viscous forces acting on the unit shell area. This relation is taken into account in the secular linear equations obtained in Sec. III [system (23) and Eq. (26)]. The resulting (inhomogeneous) linear system relates the exciting force and the displacement field amplitudes,

$$M_{11}A_{lm}^Y + M_{12}A_{lm}^Z = F_\perp^0 Y_{lm}^*(\Omega^0)/R^2,$$

$$M_{21}A_{lm}^Y + M_{22}A_{lm}^Z = F_\|^0\big[\mathbf{N}\mathbf{Z}_{lm}^*(\Omega^0)\big]/R^2,$$

$$M_{33}A_{lm}^W = F_\|^0\big[\mathbf{N}\mathbf{W}_{lm}^*(\Omega^0)\big]/R^2. \quad (32)$$

Here $M_{ij} = L_{ij} + Q_{ij}$ for $i,j < 3$ and $M_{33} = \mu(l-1)(l+2)/R^2 - i\omega[\eta_{\mathrm{in}}(l-1) + \eta_{\mathrm{out}}(l+2)]/R$.

The amplitudes A_{lm}^Y, A_{lm}^Z, and A_{lm}^W obtained from system (32) determine the displacement amplitude $\mathbf{A}(\Omega)$ for all points located on the sphere surface. Namely, the amplitude of the PP displacement is

$$\mathbf{A}(\Omega_0) = \sum_{l=1}^{l=l_{\max}} \sum_{m=-l}^{m=l} [A_{lm}^Y Y_{lm}(\Omega_0)\mathbf{e}_r + A_{lm}^Z \mathbf{Z}_{lm}(\Omega_0) \\ + A_{lm}^W \mathbf{W}_{lm}(\Omega_0)]. \quad (33)$$

Due to the finite PP radius R_p, the modes with $l \geq 2\pi R/R_p$ cannot contribute to the PP motion. Therefore, a cutoff of high-order harmonics has been carried out.

To calculate the radial response function $\alpha_\perp$, we put $F_\|^0 = 0$ in system (32). Then, using the relation

$$\sum_{m=-l}^{m=l} Y_{lm}(\Omega^0) Y_{lm}^*(\Omega^0) = (2l+1)/(4\pi) \quad (34)$$

(which is invariant with respect to the PP position), one can take a sum over equivalent modes and obtain

$$\alpha_\perp = \sum_{l=1}^{l_{\max}} \frac{(2l+1)M_{22}}{4\pi R^2 D}, \quad (35)$$

where D is the determinant of matrix $\hat{L} + \hat{Q}$.

Analogously, to calculate the tangent response function $\alpha_\|$ we substitute in Eq. (32) $F_\perp^0 = 0$. To take a sum over the modes, we use the following property of vector spherical harmonics:

$$\sum_{m=-l}^{m=l} \big[\mathbf{V}_{lm}(\Omega^0)\mathbf{N}\big]\big[\mathbf{V}_{lm}^*(\Omega^0)\mathbf{N}\big] = (2l+1)/(8\pi), \quad (36)$$

where $\mathbf{V}_{lm}$ is $\mathbf{Z}_{lm}$ or $\mathbf{W}_{lm}$. Finally, the in-plane response function reads

$$\alpha_\| = \sum_{l=1}^{l_{\max}} \frac{(2l+1)M_{11}}{8\pi R^2 D} \\ + \sum_{l=1}^{l_{\max}} \frac{2l+1}{8\pi\big\{\bar{\mu}(l-1)(l+2) - i\omega R[\eta_{\mathrm{in}}(l-1) + \eta_{\mathrm{out}}(l+2)]\big\}}. \quad (37)$$

The first sum in Eq. (37) expresses the contribution from the coupled bending and stretching modes. The second one corresponds to the contribution induced by the shear mode. Since the bending mode in the spherical geometry (contrary to the planar one) involves the inplane displacements, the first sum in Eq. (37) does not disappear even in the $\lambda \to \infty$ limit of an incompressible membrane.

Let us stress that the known response functions of the flat membrane [16] can be easily reproduced from Eqs. (35) and (37). For that goal, it is sufficient to replace the sums in Eqs.

(35) and (37) by integrals over the wave vector $q(l = qR; q_{max} = l_{max}/R)$ and then to take the $R \to \infty$ limit. For practical comparison, we present here the known out-of-plane and in-plane response functions [16] for the FM in the following form:

$$\alpha_\perp^{FM} = \int_{q=0}^{q_{max}} \frac{dq}{2\pi(\bar{K}q^3 - 2i \sum \eta \omega)}, \qquad (38)$$

$$\alpha_\parallel^{FM} = \int_{q=0}^{q_{max}} \frac{dq}{4\pi((\bar{\lambda} + 2\bar{\mu})q - 2i \sum \eta \omega)}$$

$$+ \int_{q=0}^{q_{max}} \frac{dq}{4\pi(\bar{\mu}q - i \sum \eta \omega)}, \qquad (39)$$

where $\sum \eta = \eta_{in} + \eta_{out}$ and the first and second parts of Eq. (39) represent the contributions of the stretching and shear modes, respectively.

Along the same lines, one can obtain the two-particle correlation function. It is usually calculated to fit microrheological data in one of the more important cases when two PP's are embedded in the opposite points of the spherical vesicle and time dependencies of both particle displacements are registered simultaneously. Due to the symmetry of the problem, the radial motion of the first PP cannot correlate with the tangent motion of the second PP. In addition, the mutually perpendicular tangent motions of the PP's are not correlated. Therefore, as in the previous case, the two-particle correlation function has only two nonzero components. Through the fluctuation-dissipation theorem, this function can be written in terms of the imaginary part of the two-point response function $\alpha_i'(\omega)$,

$$\langle S_i(\omega) \rangle = 2 \, \text{Im}[\alpha_i'(\omega)] k_B T / \omega. \qquad (40)$$

The response α_i' determines the amplitude $A_i'(\omega)$ of the first PP displacement when the exciting force $F_i = F_i^0 \exp(i\omega t)$ is applied to the second PP: $\alpha_i' = A_i'/F_i^0$. Using the known parity of Y_{lm} functions, one can easily modify relation (34),

$$\sum_{m=-l}^{m=l} Y_{lm}(\Omega^0) Y_{lm}^*(\Omega^1) = (-1)^l (2l+1)/(4\pi), \qquad (41)$$

where Ω^0 and Ω^1 are two opposite points on the sphere. Then summing over equivalent modes, we obtain the radial two-point response function,

$$\alpha_\perp' = \sum_{l=1}^{l_{max}} (-1)^l \frac{(2l+1)M_{22}}{4\pi R^2 D}. \qquad (42)$$

Similar calculation gives the form of the tangent two-point response function,

$$\alpha_\parallel' = \sum_{l=1}^{l_{max}} (-1)^l \left[\frac{(2l+1)M_{11}}{8\pi R^2 D} - \frac{2l+1}{8\pi\{\bar{\mu}(l-1)(l+2) + i\omega R[\eta_{in}(l-1) + \eta_{out}(l+2)]\}} \right]. \qquad (43)$$

Different signs of the terms in the square brackets are related to the different parity of functions $\mathbf{Z}_{lm}$ and $\mathbf{W}_{lm}$.

Experimental power spectra usually being discussed in terms of an incompressible shell, we consider in the last part of this section response functions (35) and (37) in the $\lambda \to \infty$ limit. Besides, the viscosities of the inner and outer liquids are taken equal: $\eta_{in} = \eta_{in} = \eta$. These simplifications permit easier comparison of the response functions of the spherical shell with those of the flat membrane. The comparison is done for the low-frequency region of the spectrum. In this region, the contribution of modes with small wave number becomes more important. At small wave numbers, the sperical geometry influences strongly the dynamics of the shell and consequently its response.

The incompressibility condition leads to the following simplification of Eqs. (35), (37), and (39). (i) The first term of Eq. (39) (related to the stretching mode) tends to zero. (ii) Out-of-plane response function (35) takes the form

$$\alpha_\perp = \sum_{l=1}^{l_{max}} \frac{R^2(2l+1)l(l+1)}{4\pi X}, \qquad (44)$$

where $X = 4R^2\bar{\mu}(l-1)(l+2) + \bar{K}(l+2)^2(l+1)l(l-1)^2 - i\omega\eta R^3(2l+1)(2l^2+2l-1)$. As one can expect, the equation $X=0$ is equivalent to dispersion relation (27). (iii) The first term in Eq. (37) is simplified and the in-plane response transforms into the form

$$\alpha_\parallel = \sum_{l=1}^{l_{max}} \frac{R^2(2l+1)}{2\pi X} + \sum_{l=1}^{l_{max}} \frac{2l+1}{8\pi[\bar{\mu}(l-1)(l+2) - i\omega\eta R(2l+1)]}. \qquad (45)$$

The two-point response functions for the incompressible shell (42) and (43) are calculated analogously.

In the limit case under consideration, the stretching mode is impossible and the first term in Eq. (45) represents the bending mode contribution only. Let us stress that there exist two main points of difference between the responses of the FM and those of the spherical shell. Both of them are much more pronounced in the low-frequency region. First, since the bending mode in the spherical shell always possesses an in-plane polarization component, the in-plane response of the spherical shell is greater than that of the FM. Second, due to the shear elasticity of the spherical shell, its out-of-plane response is essentially smaller than that of the FM. The contribution of the shear modulus $\bar{\mu}$ [see the denominator in Eq. (44)] renormalizes the effective value of $\bar{K}$, especially for small numbers l.

One can make the following estimation of the frequency region where the response functions of the spherical shell can be well approximated by those of the FM. Let us analyze

first the radial response (44). We are looking for the frequency region where sum (44) can be approximated by integral (38). For this purpose, one should first replace the wave vector q in Eq. (38) by l/R, where l is the wave number and R is the radius, and then transform Eq. (38) into a sum,

$$\alpha_\perp^{FM} = \sum_{l=1}^{l_{max}} \frac{1}{2\pi R \left[\bar{K}(l/R)^3 - 4i\eta\omega \right]}. \qquad (46)$$

At big wave numbers $(l \gg 1)$, the terms of sum (46) are very close to the corresponding terms in sum (44) and do not limit the region of the FM model validity. At small wave numbers $(l \sim 1)$, the terms in Eq. (46) become close to those in Eq. (44) in the region where

$$\omega \gg \frac{|R^2 \bar{\mu} + \bar{K}|}{\eta R^3}. \qquad (47)$$

Along the same lines, the analogous consideration of in-plane responses (45) and (39) shows that in addition to condition (47), the frequency should also satisfy

$$\omega \gg \frac{|\bar{\mu}|}{\eta R}. \qquad (48)$$

Figure 3 is devoted to a comparison of response functions discussed in this section. Let us stress that the order of magnitude of material constants used to plot this figure is one of possible orders for viscoelastic biological membranes. It is possible to increase significantly the difference between the curves corresponding to the FM and to the spherical shell using other material constants. Unfortunately, because of the trapping of the PP's attached at the opposite sides of the CV [6], the low-frequency limit of the experimental power spectra cannot be related to the theoretical power spectra of the free CV. Correct comparison with available experimental data on actin-coated vesicles is possible only for the region of ω where the trapping influence on the CV dynamics is negligible. This will be the aim of the following section.

VI. FITTING OF THE EXPERIMENTAL DATA AND DISCUSSION

In this section, we estimate the material constants of the actin-coated CVs using their known experimental power spectra [6,7]. Two different fits of the spectra are compared: (i) using the response functions of the FM model which neglects the curvature of CVs [see Eqs. (38) and (39)] and (ii) in the frame of the proposed approach which takes into account the spherical geometry of the vesicle. For numerical fitting of the power spectra, we consider the shell response in the $\lambda \to \infty$ limit.

Following [6,7,16], and references therein, we assume that in the $\omega \gg 1 \text{ s}^{-1}$ region the viscoelastic moduli scale as

$$G^j(\omega) = G_0^j (-i\omega/\omega_0)^{\gamma_j}, \qquad (49)$$

where $\omega_0 = 1 \text{ s}^{-1}$ and G_0^j is a real positive constant. Let us stress that the above equation can be a good approximation to the frequency dependence of the elastic moduli only for
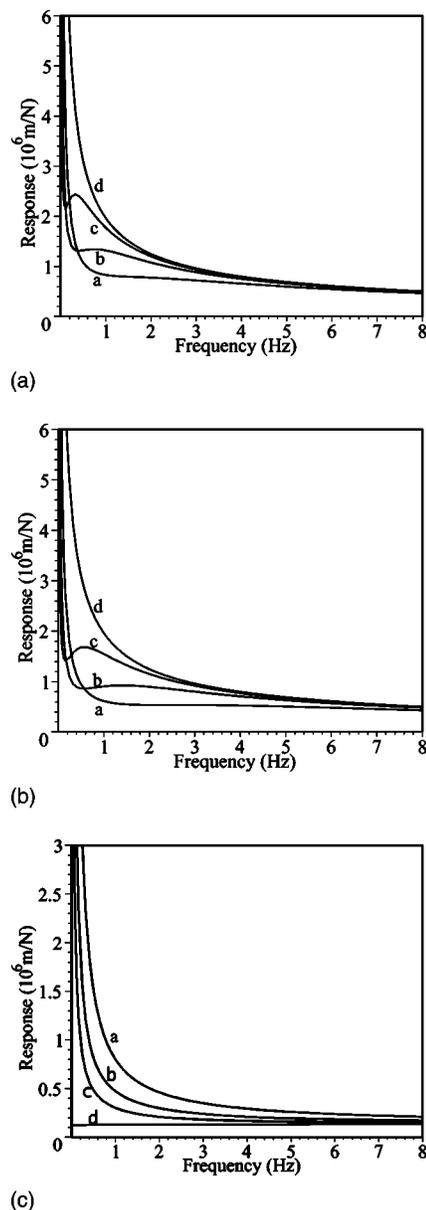

(a)

(b)

(c)

FIG. 3. Imaginary parts of the response functions calculated for the incompressible flat and spherical membranes. Panels (a) and (b) show radial responses and panel (c) shows tangent ones. Curves (a)–(c) represent the responses of spherical shells with increasing radius for the fixed size of PP. The response of the flat membrane is given by curve (d). We take $\eta = 10^{-3}$ Pa s. The radii R for curves (a)–(c) are $R_a = 2 \times 10^{-5}$ m, $R_b = 4 \times 10^{-5}$ m, and $R_c = 8 \times 10^{-5}$ m. Since the PP size R_P is constant, the cutoff number l_{max} is proportional to the membrane radius. For curves (a)–(c), l_{max} is taken equal to 100, 200, and 400, respectively. For the flat membrane $q_{max} = l_{max}/R$. The values of the material constants used to plot the curves in panels (a) and (c) are as follows: $\bar{K} = 10^{-18} - i(\omega/\omega_0)10^{-20}$ J and $\bar{\mu} = 10^{-6} - i(\omega/\omega_0)10^{-9}$ N/m, where $\omega_0 = 1 \text{ s}^{-1}$. For plots in panel (b), the shear modulus $\bar{\mu}$ is taken two times greater. This increases the difference between radial responses of spherical and flat membranes (see in the text). At small wave numbers, the spherical geometry influences strongly the membrane dynamics, therefore the difference between the response functions increases in the low-frequency region.
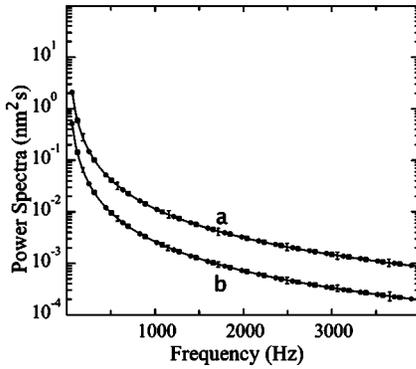
FIG. 4. In-plane (a) and out-of-plane (b) power spectra of the actin-coated vesicle. Solid lines approximate the average experimental spectral density from Ref. [6]. Error bars show the uncertainty in the experimental power spectra. Circles and squares represent theoretically calculated power spectra for the flat membrane and spherical shell models, respectively. The accuracy of the fits is high enough and the difference between experimental and theoretical curves in both cases is much smaller than the width of the solid lines. Nevertheless, the values of material constants extracted from the power spectra in the frame of the spherical shell model are different from those obtained in the frame of the flat membrane model (see in the text).

real ω, for example for the case of stationary oscillation of a viscoelastic solid under the influence of a periodic exciting force. As it is easy to check for both FM and spherical shell models, relation (49) does not lead to physically reasonable eigenrelaxation frequencies. To make this fact obvious, it is sufficient to substitute (49) into equations of motion of Ref. [16] or of the present work [see, for example, the simplest case of the shear mode given by Eq. (26)]. Note that the eigenrelaxation frequencies are imaginary negative values and the imaginary part of G^j moduli for the stationary oscillating system has a negative sign [both of these facts follow from the time dependence of expressions (12) and (15)]. Otherwise, the vibration amplitude would grow infinitely with time. Fortunately, the computation of the power spectra on the basis of the fluctuation-dissipation theorem does not imply an explicit knowledge of the eigenrelaxation frequencies. Besides, the variable ω in all response functions (needed for the power spectra computation) and in Eq. (28) has a real value making assumption (49) acceptable. Therefore, we fit experimental data using Eq. (49) in the following explicit form [6]: $\bar{K} = K_0(\omega/\omega_0)^\alpha[1 - i\tan(\pi\alpha/2)]$ and $\bar{\mu} = \mu_0(\omega/\omega_0)^\beta[1 - i\tan(\pi\beta/2)]$, respectively.

In the frequency range from $f = 60$ Hz to $f = 4000$ Hz, one can approximate the experimental in-plane and out-of-plane power spectra of the actin-coated CV (see Fig. 2 and Fig. 3 in Ref. [6]) by the equations $2K_BT0.185 \times 10^8(\omega/\omega_0)^{-1.87}[\text{m}^2\text{s}]$ and $2K_BT0.44 \times 10^7(\omega/\omega_0)^{-1.88}[\text{m}^2\text{s}]$, respectively (see Fig. 4). For the vesicle radius equal to 2×10^{-5} m and for the PP one equal to 10^{-6} m, we estimate the cutoff l_{max} as 120. The numerical fitting of the power spectra calculated using the fluctuation-dissipation theorem

in terms of functions (44) and (45) yields $K_0 = 18 \times 10^{-19}$ J, $\alpha = 0.66$, $\mu_0 = 0.70 \times 10^{-8}$ N/m, and $\beta = 0.79$. Fitting in the frame of the FM model [using functions (38) and (39)] gives $K_0 = 30 \times 10^{-19}$ J, $\alpha = 0.63$; $\mu_0 = 0.65 \times 10^{-8}$ N/m, $\beta = 0.79$. One can roughly estimate the uncertainty of α and β determination (related to the uncertainty in the experimental data) as a few percent. The uncertainty in K_0 and μ_0 determination is one order of magnitude greater.

As far as we know, no experimental data on the two-particle correlation functions in actin-coated vesicles are available at present. Nevertheless, it seems useful to compute these functions using material constants obtained above by fitting the spectra in terms of functions (44) and (45). In the frequency region 60–4000 Hz, the resulting functions $S_\parallel(\omega)$ and $S_\perp(\omega)$ are well approximated by expressions $-2K_BT1.10 \times 10^6(\omega/\omega_0)^{-1.99}[\text{m}^2\text{s}]$ and $-2K_BT1.60 \times 10^6(\omega/\omega_0)^{-2.00}[\text{m}^2\text{s}]$, respectively. It is interesting to note that both functions scale with frequency as ω^{-2} like the power spectrum of a simple Brownian motion.

Let us discuss what happens to the one-point response functions and to the fits of the spectra when the PP radius is changed. In the theory under consideration, this variation changes l_{max} (or q_{max}) value. For PP size larger than that taken earlier in this section and corresponding, for example, to $l_{max} = 100$, the above K_0 and α values are preserved and the shear modulus change is very small. For the spherical and planar geometry, we have calculated $\mu_0 = 0.71 \times 10^{-8}$ N/m and $\mu_0 = 0.66 \times 10^{-8}$ N/m, respectively, whereas $\beta = 0.78$ in both cases. In the constant extraction procedure, the shear modulus value is more sensitive to the PP radius variation since the corresponding response function diverges in the $l_{max} \to \infty$ limit. The β value obtained is close to the earlier experimental results for a bulk solution of actine filaments [24] confirmed by a theoretical calculation of $\beta = 0.75$ [25] but differs from that given in Ref. [6]. Also let us note that the widely cited statement that the in-plane spectrum scales with the frequency as $(\omega/\omega_0)^{-\beta-1}$ is rather approximate.

The fits of power spectra presented in this section concern only the intermediate-frequency region (60–4000 Hz). In the higher-frequency region, from an experimental point of view, the modes cannot be thermally activated, and from a model point of view, the inertial term in the Navier-Stokes equation cannot be omitted. In the lower-frequency region, which is the most interesting for the studies of biological and biomimetic matter, one experimental problem arises. The trapping of PPs attached at opposite sides of the CVs modifies strongly the intrinsic spectra of the shell. To get the information about low-frequency dynamics of CVs, another experimental technique is needed. By contrast, the fit of the spectra in this region is simpler since Eq. (49) is not applicable, real parts of elastic moduli are practically constant, and imaginary parts are linear in ω. Let us finally note that in the low-frequency region, the FM model is no longer reliable for the material constants extraction since at small wave numbers the spherical geometry strongly influences the membrane dynamics (see the end of Sec. V). Though in the intermediate-frequency region the difference between the constants values obtained from the FM and spherical shell

models does not exceed 50%, in the low-frequency region it can be significantly greater.

VII. SUMMARY

In conclusion, let us briefly enumerate the main results and features of the proposed approach. We develop the theory of the overdamped linear dynamics of the composite spherical vesicle embedded in a viscous Newtonian fluid and discuss its relation to microrheological measurements. The elastic energy of the vesicle is characterized by in-plane shear and stretching moduli and by bending rigidity. Finite nonzero shear elasticity of the CVs makes the dynamics of the viscoelastic spherical shell considered in this paper quite different with respect to the linear dynamics of nearly spherical fluid vesicles developed in [10–12]. We argue that a purely geometrical understanding of the shell incompressibility adopted in fluid vesicles studies should be replaced in this case by the physical incompressibility condition which consists in local mass density conservation.

We pay particular attention to the influence of spontaneous curvature on the viscoelastic vesicle dynamics. Contrary to case of the FM model [16], spherical geometry of the shell permits linear coupling between bending and stretching relaxation modes. We show that in the limit case of an incompressible vesicle, the bending mode contains both radial and tangent components with amplitude ratio dependent on the wave number. To relate the spherical shell model to microrheological data, we calculate the fluctuation spectrum of a rigid PP embedded in the CV. The role of curvature becomes important in the physical processes, with the main contributions coming from small wave numbers. We show that planar geometry can be used instead of a spherical one only in the region where the effective wave number $l=qR$ satisfies to the condition $qR \gg 1$. In particular, the response functions of the incompressible FM can replace those of the incompressible spherical vesicle in the frequency region where both conditions (47) and (48) are satisfied.

The response functions which determine the fluctuation spectrum are compared with those of the FM model. Since the bending mode in the spherical shell always has the in-plane component, the in-plane response of the spherical shell is greater than that of the FM. On the contrary, due to the shear elasticity of the spherical shell, its out-of-plane response is smaller than that of the FM. To complete the analysis, we compute also the correlated fluctuation spectrum of two particles embedded in the vesicle in two opposite points.

In the same spirit of comparison, we estimate material constants for actin-coated vesicles from known experimental data [6–8] using the fits (i) by the spherical shell model and (ii) by the FM model. In the frequency range 60–4000 Hz, the difference between the values obtained by two fits does not exceed 50%. However, in the low-frequency region the reliable material constants can be obtained only in the model with nonzero spontaneous curvature.

The extension of this work can be done in several directions. Our results can be applied to the vesicles coated with crystallized proteines or biological filaments, to giant polymerosomes and, to a certain extent, to living cell. To be closer to the complex dynamical behavior of biological and bio-mimetic objects, the model can take into account chemical heterogeneity of the vesicles material. In the linear dynamics, the relative motion of the parts can then lead to additional types of modes. Another development of the present work can concern the influence of the shell permeability (in phospholipid vesicles and in living cells) on the relaxation rate of the modes. These issues will be addressed in a forthcoming paper. Both effects will not change qualitative conclusions of the model but can be useful for practical quantitative fits of microrheological data.

ACKNOWLEDGMENTS

APPENDIX

Normalized scalar spherical harmonics Y_{lm} span $D_l[(-1)^l]$ irreducible representations (IRs) of the sphere symmetry group O_3. For the set of Y_{lm} functions, this normalization means that $\int\int Y_{lm}Y_{pq}^* \sin\theta d\theta d\phi = \delta_{lp}\delta_{mq}$. The normalized Y_{l0} function is $\sqrt{(2l+1)/(4\pi)}P_l(\cos\theta)$, where P_l is the Legendre polynomial of the lth order.

Vector spherical harmonics $\mathbf{Z}_{lm}$ and $\mathbf{W}_{lm}$ spanning the in-plane displacement field of the spherical shell are less known. They are two-dimensional vector functions with θ and ϕ components. Functions $\mathbf{Z}_{lm}$ describe the shell stretching and span the same sequence $D_l[(-1)^l]$ of the IRs as functions Y_{lm} do. They are normalized in the following way: $\int\int \mathbf{Z}_{lm}\mathbf{Z}_{pq}^* \sin\theta d\theta d\phi = \delta_{lp}\delta_{mq}$. Functions $\mathbf{W}_{lm}$ which are normalized analogously describe the shear deformation of the shell. They span $D_l[(-1)^{(l+1)}]$ IRs of the sphere symmetry group. The functions $\mathbf{W}_{l0}$ and $\mathbf{Z}_{l0}$ preserve the rotational symmetry around the z direction like Y_{l0} does and, with respect to the functions with $m \neq 0$, have a simpler form. Two components (θ and ϕ) of the normalized vector function $\mathbf{Z}_{l0}$ are $\partial_\theta Y_{l0}/\sqrt{l(l+1)}$ and 0, respectively. Analogously, the normalized $\mathbf{W}_{l0}$ function is equal to $(0, \partial_\theta Y_{l0}/\sqrt{l(l+1)})$. Functions $\mathbf{W}_{lm}$ and $\mathbf{Z}_{lm}$ with $m > 0$ can be obtained from the functions with $m = 0$ using the elevating operator [20]. It is simpler to perform this procedure for the displacement field described in the Cartesian coordinate system. In such a case, $\mathbf{Z}_{l0}$ and $\mathbf{W}_{l0}$ functions take the form $\mathbf{Z}_{l0} = \{\mathbf{e}_3 \sin(\theta) - \cos(\theta)[\mathbf{e}_1 \cos(\phi) + \mathbf{e}_2 \sin(\phi)]\}\partial_\theta Y_{l0}/\sqrt{l(l+1)}$ and $\mathbf{W}_{l0} = [\mathbf{e}_1 \sin(\phi) - \mathbf{e}_2 \cos(\phi)]\partial_\theta Y_{l0}/\sqrt{l(l+1)}$, where $\mathbf{e}_j$ are the Cartesian basis vectors. The corresponding elevating operator reads

$$L_+ = \exp(i\phi)[\partial_\theta + i\,\mathrm{ctg}(\theta)\partial_\phi] + \mathbf{e}_3(\mathbf{e}_1 + i\mathbf{e}_2) - (\mathbf{e}_1 + i\mathbf{e}_2)\mathbf{e}_3.$$

(A1)

Operator action consists in $L_+\mathbf{Z}_{lm} = [(l+m+1)(l-m)]^{(1/2)}\mathbf{Z}_{l,m+1}$. Triple products $\mathbf{e}_l\mathbf{e}_m\mathbf{e}_n$ resulting from the operator action are equal to $\mathbf{e}_l\delta_{mn}$. The operator L_+ also elevates $\mathbf{W}_{lm}$ functions. Functions with negative m are obtained by the complex conjugation of those with positive m.

[1] B. Alberts *et al.*, *Molecular Biology of the Cell* (Garland, New York, 1994).

[2] F. Brochard and J. F. Lennon, J. Phys. (Paris) **36**, 1035 (1975).

[3] E. A. Evans, Biophys. J. **13**, 941 (1973); **16**, 597 (1976).

[4] R. E. Waugh, Biophys. J. **70**, 1027 (1996).

[5] P. Ratanabanankoon *et al.*, Langmuir **19**, 1054 (2003).

[6] E. Helfer, S. Harlepp, L. Bourdieu, J. Robert, F. C. MacKintosh, and D. Chatenay, Phys. Rev. Lett. **85**, 457 (2000).

[7] E. Helfer, S. Harlepp, L. Bourdieu, J. Robert, F. C. MacKintosh, and D. Chatenay, Phys. Rev. E **63**, 021904 (2001).

[8] E. Helfer, S. Harlepp, L. Bourdieu, J. Robert, F. C. MacKintosh, and D. Chatenay, Phys. Rev. Lett. **87**, 088103 (2001).

[9] D. E. Discher, N. Mohands, and E. A. Evans, Science **266**, 1032 (1994).

[10] M. B. Schneider, J. T. Jenkins, and W. W. Webb, J. Phys. (Paris) **45**, 1457 (1984).

[11] S. T. Milner and S. A. Safran, Phys. Rev. A **36**, 4371 (1987).

[12] U. Seifert, Eur. Phys. J. B **8**, 405 (1999).

[13] L. Landau and E. Lifchitz, *Theory of Elasticity* (Mir, Moscow, 1983).

[14] Z. Zhang, H. T. Davis, and D. M. Kroll, Phys. Rev. E **48**, R651 (1993).

[15] H. Yoon and J. M. Deutsch, Phys. Rev. E **56**, 3412 (1997).

[16] A. J. Levine and F. C. MacKintosh, Phys. Rev. E **66**, 061606 (2002).

[17] L. I. Sedov, *Mechanics of Continuous Media, Series in Theoretical and Applied Mechanics* (World Scientific, Singapore, 1997).

[18] B. Dubrovin, S. Novikov, and A. Fomenko, *Modern Geometry, Graduate Texts in Mathematics*, 2nd ed. (Springer-Verlag, New York, 1992).

[19] G. Lim, M. Wortis, and R. Mukhopadhyay, Proc. Natl. Acad. Sci. U.S.A. **99**, 16 766 (2002).

[20] J. P. Elliot and P. G. Dawber, *Symmetry in Physics* (The Macmillan Press Ltd., London, 1979).

[21] L. D. Landau and E. M. Lifchitz, *Hydrodynamics* (Pergamon, New York, 1981).

[22] H. Lamb, *Hydrodynamics*, 6th ed. (Cambridge University Press, Cambridge, 1932).

[23] P. Lenz and D. R. Nelson, e-print cond-mat/0211140.

[24] F. Gittes, B. Schnurr, P. D. Olmsted, F. C. MacKintosh, and C. F. Schmidt, Phys. Rev. Lett. **79**, 3286 (1997).

[25] D. C. Morse, Phys. Rev. E **58**, R1237 (1998).